

Simulation of the diurnal cycle in a climate model and its evaluation using data from Meteosat 7

By A. SLINGO*, K. I. HODGES and G. J. ROBINSON
Environmental Systems Science Centre, University of Reading, UK

(Received 26 August 2003; revised 12 January 2004)

SUMMARY

The representation of the diurnal cycle in the Hadley Centre climate model is evaluated using simulations of the infrared radiances observed by Meteosat 7. In both the window and water vapour channels, the standard version of the model with 19 levels produces a good simulation of the geographical distributions of the mean radiances and of the amplitude of the diurnal cycle. Increasing the vertical resolution to 30 levels leads to further improvements in the mean fields. The timing of the maximum and minimum radiances reveals significant model errors, however, which are sensitive to the frequency with which the radiation scheme is called. In most regions, these errors are consistent with well documented errors in the timing of convective precipitation, which peaks before noon in the model, in contrast to the observed peak in the late afternoon or evening. When the radiation scheme is called every model time step (half an hour), as opposed to every three hours in the standard version, the timing of the minimum radiance is improved for convective regions over central Africa, due to the creation of upper-level layer-cloud by detrainment from the convection scheme, which persists well after the convection itself has dissipated. However, this produces a decoupling between the timing of the diurnal cycles of precipitation and window channel radiance. The possibility is raised that a similar decoupling may occur in reality and the implications of this for the retrieval of the diurnal cycle of precipitation from infrared radiances are discussed.

KEYWORDS: Diurnal cycle Satellite data Unified Model

1. INTRODUCTION

The annual and diurnal cycles represent the two strongest modes of forced, periodic variability exhibited by a wide range of atmospheric and surface variables. The ability to represent the annual cycle, as well as interannual and longer term changes, provides an important test of climate model performance and is often used to evaluate models (Gates *et al.* 1999). On the other hand, relatively few studies have examined the diurnal cycle in climate models, despite the fact that this enables the models to be tested on a timescale much closer to that of many important atmospheric physical processes, such as clouds and convection. One reason may be the intense present-day interest in modelling climate change and variability on interannual to decadal timescales (e.g. IPCC 2001), which inevitably requires the model output to be averaged over periods of at least one month, erasing information on the high-frequency behaviour. However, as will be shown later, this behaviour provides clues as to the processes responsible for some persistent model systematic errors, and may thus help to improve the models and increase the confidence in climate predictions.

Several studies have shown that infrared window channel observations from geostationary meteorological satellites can be used to infer a great deal of information on the diurnal cycle of land surface temperatures, clouds and convection (e.g. Duvel and Kandel 1985; Yang and Slingo 2001 (hereafter referred to as YS), and references therein). Additionally, observations in the 6.7 μm water vapour channel have been used to study the relationship between the diurnal cycle of upper tropospheric humidity (UTH) and convective cloudiness (Soden 2000). Diurnal variations are particularly large over land at low latitudes throughout the year and in midlatitudes in summer. More subtle variations over the oceans are usually believed to be caused by the absorption of solar radiation within the atmosphere (e.g. Janowiak *et al.* 1994), although significant

* Corresponding author: ESSC, University of Reading, PO Box 238, Earley Gate, Reading, Berkshire RG6 6AL, UK. e-mail: as@mail.nerc-essc.ac.uk

diurnal variations in ocean skin temperatures can also occur in light wind conditions (Gentemann *et al.* 2003).

As noted above, there have been relatively few studies comparing the diurnal cycle in models with observations, although those studies that have been performed have often revealed significant errors. Slingo *et al.* (1987) showed that the Met Office 11-layer model reproduced many of the features seen in satellite observations of the outgoing long-wave radiation, although for cloudy regions over land there were less coherent variations than in the observations. Randall *et al.* (1991) found that the diurnal cycle in precipitation simulated by the Colorado State University model was in broad agreement with observations, although, in a later study with this model, Lin *et al.* (2000) showed that the simulation was very sensitive to the value of a parameter in the model's convection scheme. Using the numerical weather prediction model of the European Centre for Medium-range Weather Forecasts (ECMWF), Morcrette (1991) noted that deep convective clouds over land dissipate as much as six hours too early in the day. Studies with successive versions of this model have found a corresponding error in the timing of precipitation over tropical land, which peaks far too early in the day (e.g. Betts and Jakob 2002). The same error was identified by YS in simulations with version HadAM3 of the Met Office Unified Model. From this limited sample, these studies indicate that the timing of tropical convection and precipitation is particularly sensitive to details of a model's formulation and that models often fail to reproduce the observed evening maximum in cloudiness and precipitation, with the modelled maxima occurring much earlier in the day.

In the present study, we build on the analysis of HadAM3 by YS in two important ways. Firstly, a version of the model's radiation scheme that can simulate the radiances observed by satellite instruments is used to perform comparisons with data from the Meteosat 7 geostationary meteorological satellite, using a temporal resolution of half an hour. The significance of simulating radiances, using a 'model to satellite' approach (Morcrette 1991; Roca *et al.* 1997), is that it enables comparisons to be made directly with the satellite measurements, which avoids the considerable uncertainties and assumptions that are associated with indirect comparisons between derived geophysical products such as cloud cover or precipitation and the corresponding model variables. Secondly, the comparisons are performed not only for the window channel but also for the water vapour channel, which provides additional information on the model's simulation of upper tropospheric humidity.

The following section briefly describes the climate model and the Meteosat data and also discusses the methodology employed to compare the model with the data. Results for the mean fields are then presented, followed by results on the timing of the diurnal cycle and a more detailed analysis over Africa and South America. The final section summarizes the conclusions which may be drawn from this work and discusses some ideas for future investigations.

2. MODEL AND SATELLITE DATA

(a) *Model*

The simulations were performed with version HadAM3 of the atmospheric component of the Met Office Hadley Centre climate model, with the addition of a version of the model's radiation code that can simulate satellite radiances. The basic model is described by Pope *et al.* (2000) and the application of the radiance code to the simulation of data from Meteosat 7 is described by Ringer *et al.* (2003). Partially cloudy grid boxes are decomposed into a number of separate columns, following Jakob and

Klein (1999). The code takes account of both the satellite viewing geometry and the spectral passband of the instrument. The standard version of the model has a horizontal resolution of 2.5° latitude by 3.75° longitude, 19 vertical levels and a full radiation calculation is performed every 3 hours of model time. For the present study, additional integrations were run to examine the sensitivity to performing full radiation calculations every model time step (half an hour) and to increasing the vertical resolution to 30 levels, thus providing a matrix of four integrations. Calling the radiation scheme every timestep increases the run time of the model considerably, so this is not a practical option for most investigations, but in the present study it provides valuable additional information. YS found that increasing the vertical resolution made little difference to their comparisons with window channel radiances, but Pope *et al.* (2001) showed that the 30-level version produces an improved simulation of both temperature and water vapour in the upper troposphere. One objective of the present work is therefore to determine whether the improved vertical and temporal resolution impacts on the simulation of the Meteosat radiances.

The model integrations were started from a previous model dump for 1 December and run to the beginning of the following May. Detailed diagnostics on the simulation of the diurnal cycle were then added and the model was run through to September. The results shown here cover the boreal summer season (June, July and August, hereafter referred to as JJA). The sea surface temperatures used were those for 1984, although the exact year chosen has little impact on the diagnostics shown here.

(b) *Meteosat data*

Data from the Meteosat 7 imager were obtained from EUMETSAT at a temporal resolution of 30 minutes and a spatial resolution of 5 km, for June to August 2002. For comparison with the model, the data were converted from instrument counts to radiances using the calibration supplied and then reduced to the same resolution as the model. The generation of the Meteosat data on the model grid was performed by first sub-sampling the data by a factor of five. These data were then averaged to the model grid using the CLAUS software (Hodges *et al.* 2000), modified to use radiances instead of temperatures.

(c) *Analysis methodology*

The radiances from Meteosat and the radiances and other diagnostics from the model integrations were processed in an identical manner. Datasets representing the mean diurnal cycle for JJA were created by compositing the data from each source according to the Universal Time. For the half-hourly Meteosat and model data, these datasets thus contain 48 geographical distributions for each composite day. For the 3-hourly model data, there are only eight such distributions. The local times of the maximum and minimum value at each grid point were calculated by searching through these distributions and converting Universal Time to local solar time, taking into account the longitude of the grid point. This simple methodology was used because it accurately finds the local time of maximum and minimum for the strong, non-sinusoidal diurnal cycles that are typical for tropical continental regions, which is the primary focus of the current work. For noisy or weak diurnal cycles, for example over the oceans, the Fourier analysis method used by YS is more reliable, although it can distort the times of maximum and minimum over land.

The above analysis was performed on the radiances, since these represent directly the energy received by the satellite. However, for ease of display and interpretation in

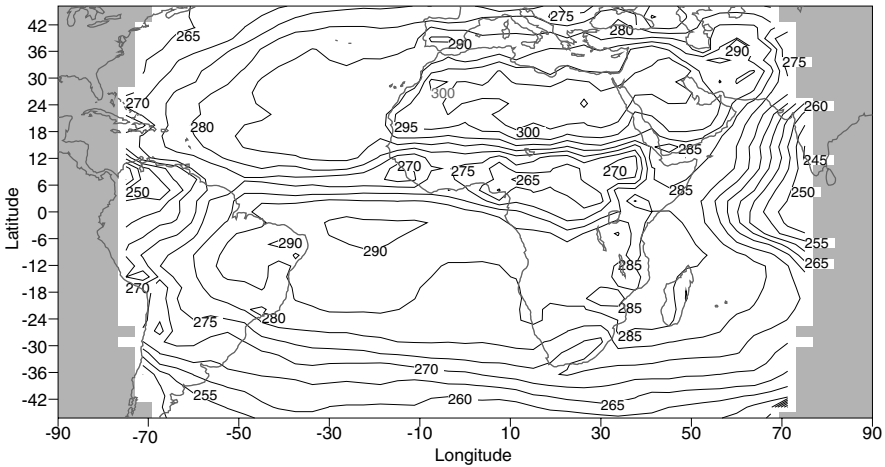


Figure 1. Mean window channel brightness temperature (K) from Meteosat 7 for June, July and August 2002.

this paper, the mean radiances from both the Meteosat data and from the model were converted to equivalent black-body brightness temperatures using the exponential fits and coefficients listed by EUMETSAT on their web site.

3. RESULTS: MEAN FIELDS

Figure 1 shows the mean window channel brightness temperatures for JJA from Meteosat. The highest values occur over the North African and Middle Eastern deserts, while the lowest values are associated with persistent deep (and hence cold) convection associated with the summer monsoons over South America, India and the Indian ocean. Weaker minima are associated with the ITCZ over tropical Africa and the Atlantic ocean. The diurnal range (Fig. 2) is largest over the deserts, associated with large surface temperature variations and clear skies. Smaller diurnal cycles are present in the ITCZ over tropical parts of Africa and of South America. Some very small, but coherent, variations are apparent over clouds above tropical parts of the Atlantic and Indian oceans, but those at higher latitudes over the oceans are not real but are due to aliasing from synoptic systems.

Differences between the simulated mean window channel brightness temperatures from the four versions of the model and those from Meteosat 7 are shown in Fig. 3. With the standard HadAM3 configuration of 19 levels and calls to the radiation every three hours, there are positive and negative differences of up to about 20K, the largest associated with a displacement of the Atlantic ITCZ to the south. The differences are reduced substantially when either the vertical resolution or the calling frequency of the radiation scheme are increased. While the statistical significance of these differences may be questionable, given that both the Meteosat data and the model simulations are for only one JJA season, the coherent and positive changes apparent in Fig. 3 suggest that these sensitivities are real. The simulated brightness temperatures are systematically 4–5 K lower than those from Meteosat, which is much greater than either the errors in the code (Ringer *et al.* 2003) or the temperature errors in the model atmosphere (Pope *et al.* 2000), suggesting that it may be due to calibration errors in the data.

The diurnal range of window channel brightness temperatures from the models (Fig. 4) compares well with that of the Meteosat data shown in Fig. 2. Note that, for

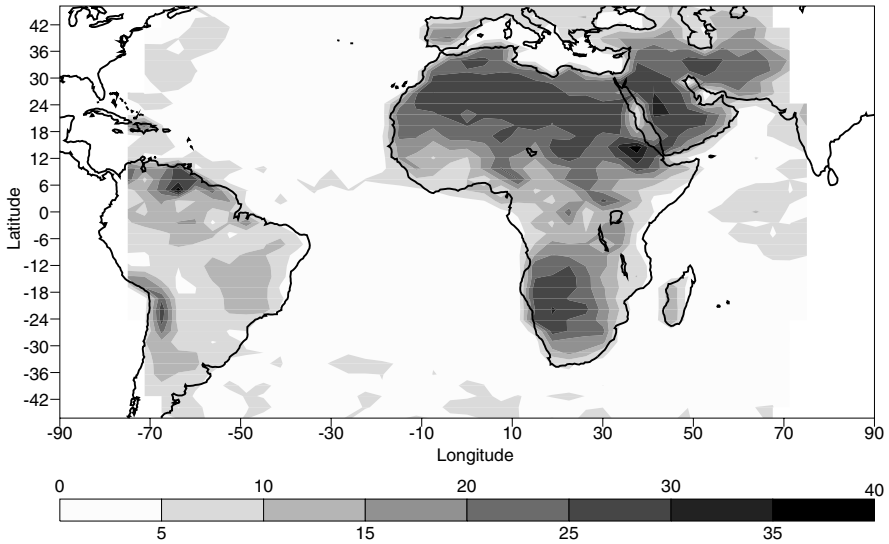


Figure 2. Diurnal range of window channel brightness temperature (K) from Meteosat 7 for June, July and August 2002.

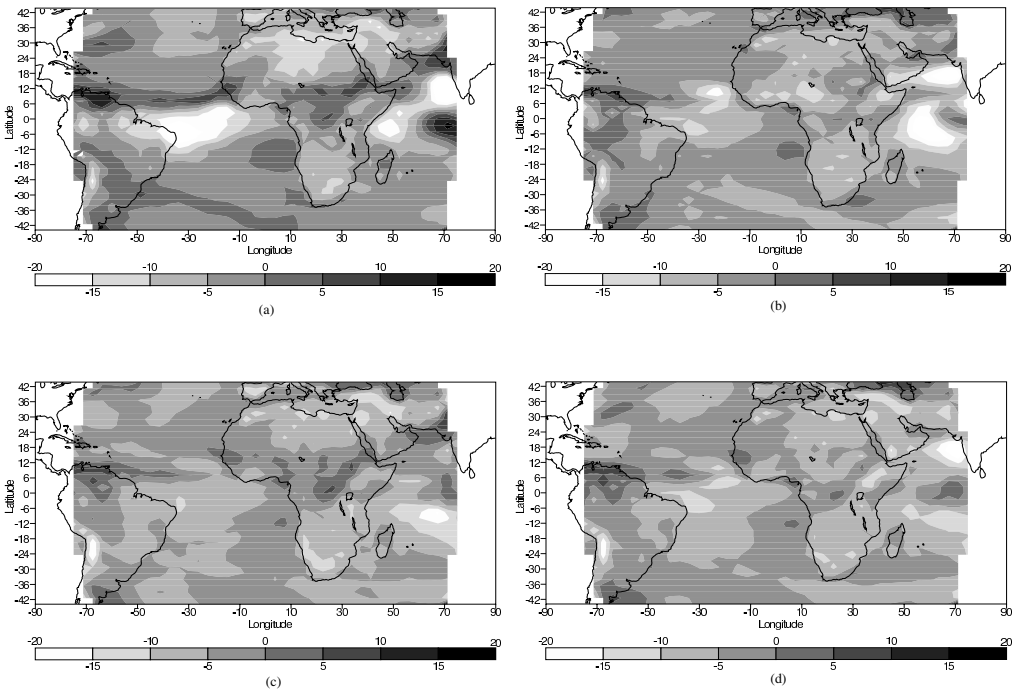


Figure 3. Mean window channel brightness temperature differences (K)—values from each of the four versions of the model minus the Meteosat values: (a) 19 levels and calls to the radiation scheme every three hours; (b) 19 levels and calls to the radiation scheme at every time step (half hour); (c) 30 levels and calls every three hours, and (d) 30 levels and calls at every time step (half hour).

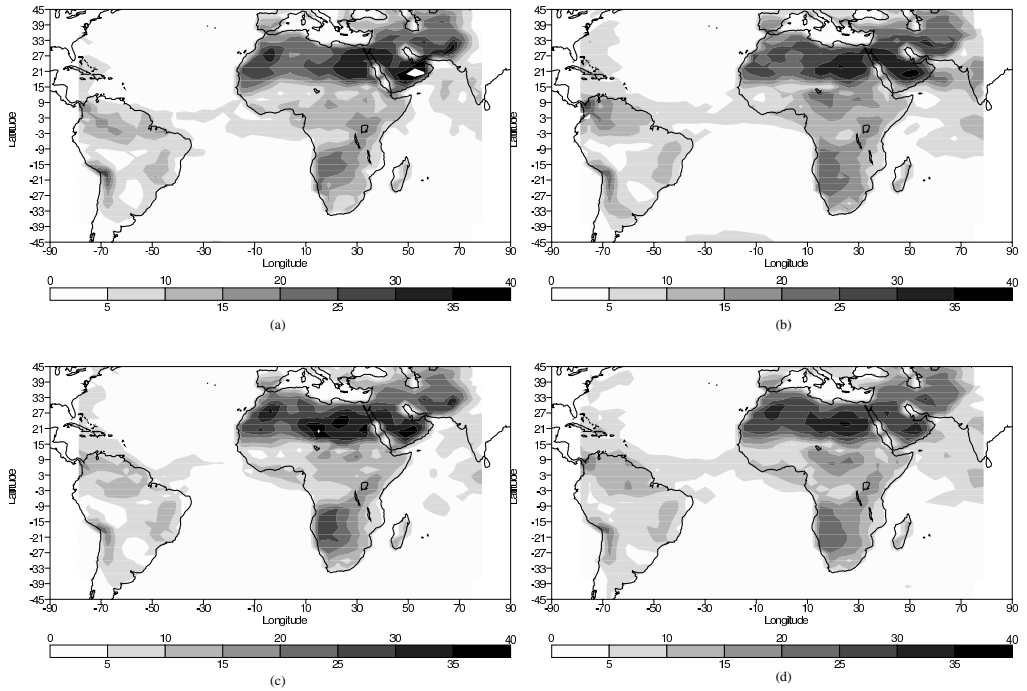


Figure 4. Diurnal range of window channel brightness temperature (K) from the four versions of the model. Panels are as in Fig. 3: (a) 19 levels and calls to the radiation scheme every three hours; (b) 19 levels and calls to the radiation scheme at every time step (half hour); (c) 30 levels and calls every three hours, and (d) 30 levels and calls at every time step (half hour).

both the data and the models, the values of diurnal range shown here are up to three times the corresponding values shown by the Fourier analysis of YS. There are two reasons for this difference. Firstly, the analysis here provides the peak-to-peak value, whereas YS show only the amplitude of the diurnal harmonic. Secondly, their figures omit the contribution from the semi-diurnal and higher frequency components, which are significant for the strongly non-sinusoidal variations over land.

Turning to the water vapour channel, the mean brightness temperatures from Meteosat 7 (Fig. 5) are lower than those in the window (Fig. 1) over the whole domain, illustrating the increased atmospheric absorption in this channel. The general structure of the two fields is quite similar, although the more prominent local minimum over the South Atlantic in the water vapour channel is a common feature in JJA, associated with strong descent and hence drying in the winter branch of the Hadley circulation. However, the pattern of the diurnal range shown in Fig. 6 is completely different from that in the window (Fig. 2). Water vapour absorption almost completely masks the surface signal that dominates the window, so the largest diurnal variations come instead from the convective clouds in the ITCZ that are deep, and hence cold enough, to be detectable above the water vapour background. While there may also be coherent diurnal variations in water vapour, these are not detectable without further analysis (Soden 2000).

The difference plots for the model (Fig. 7) again show the largest differences for the standard version of the model and reductions as the resolution is improved in both space and time. There are many similarities between the distribution shown in Fig. 7(a) and the corresponding plot by Allan *et al.* (2003) (their Fig. 4(b)), who used cloud-cleared radiances from the High-resolution InfraRed Sounder (HIRS) $6.7 \mu\text{m}$ channel

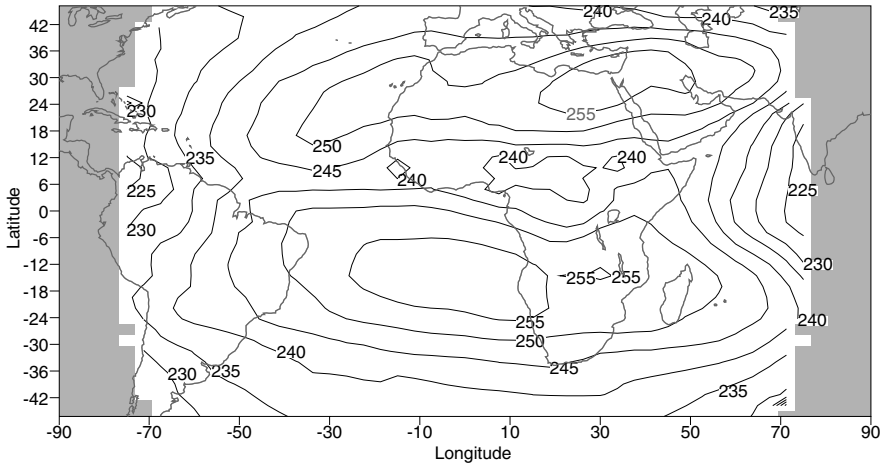


Figure 5. Mean water vapour channel brightness temperature (K) from Meteosat 7 for June, July and August 2002.

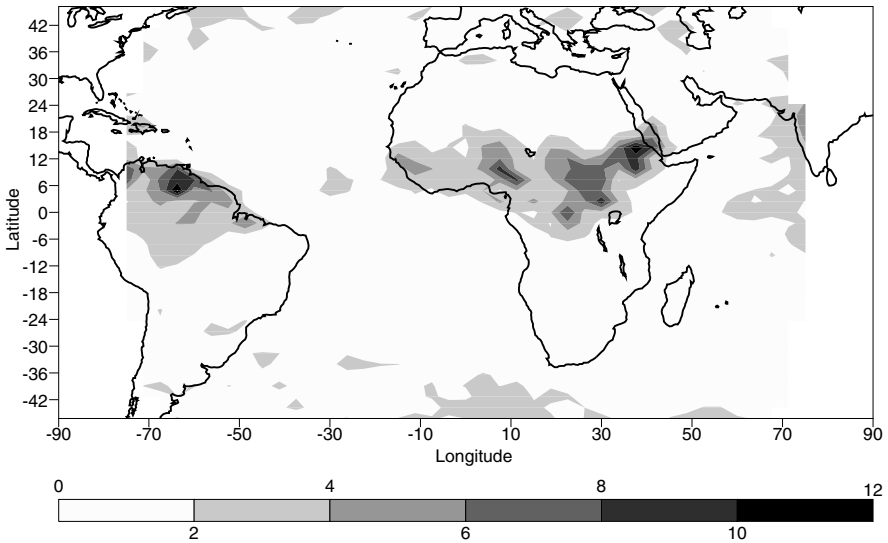


Figure 6. Diurnal range of water vapour channel brightness temperature (K) from Meteosat 7 for June, July and August 2002.

to evaluate the global moisture distribution in decadal integrations of HadAM3. This suggests that the major features apparent in Fig. 7 are caused by variations in upper tropospheric humidity, so that the reduction in the amplitude of the differences with increased resolution indicates an improved moisture distribution. The positive impact of additional vertical resolution is particularly striking, suggesting that the distribution of upper tropospheric humidity is improved, which is consistent with the findings of Pope *et al.* (2001).

The diurnal range of water vapour brightness temperature from the model (Fig. 8) is in good agreement with that from Meteosat 7 (Fig. 6), with perhaps a weak dependence on the radiation calling frequency.

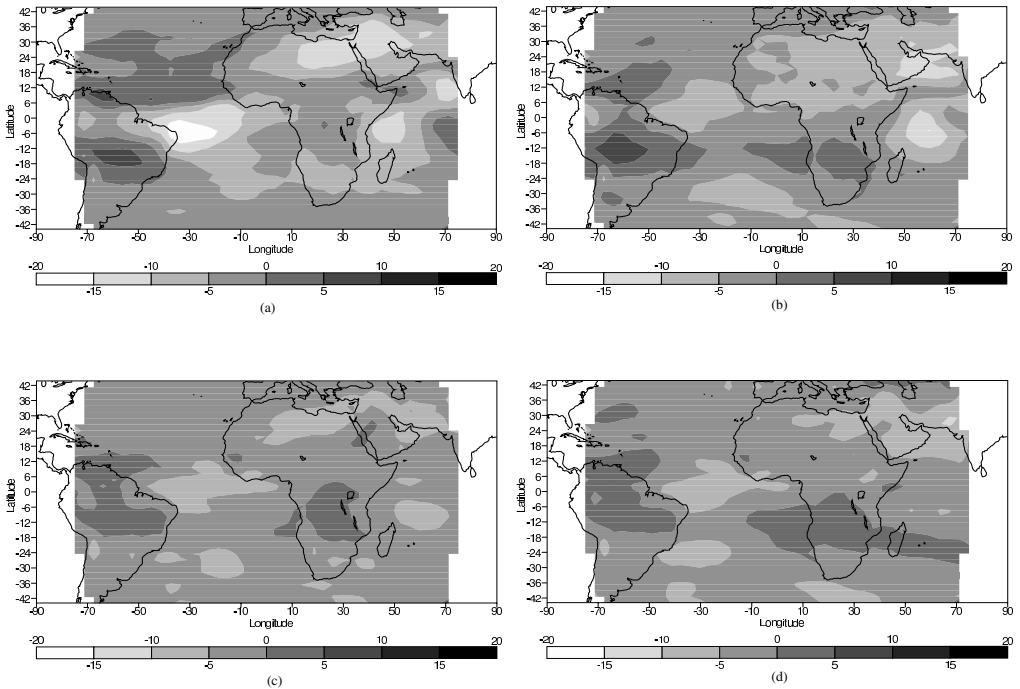


Figure 7. Mean water vapour channel brightness temperature differences (K)—values from each of the four versions of the model minus the Meteosat values. Panels are as in Fig. 3: (a) 19 levels and calls to the radiation scheme every three hours; (b) 19 levels and calls to the radiation scheme at every time step (half hour); (c) 30 levels and calls every three hours, and (d) 30 levels and calls at every time step (half hour).

4. THE PHASE OF THE DIURNAL CYCLE

We have established that the model reproduces quite well the observed mean and diurnal range of the window and water vapour channel brightness temperatures. This section examines the phase behaviour in terms of the local time of maximum and minimum radiance. The same analysis is also applied to the modelled precipitation.

The local times of maximum and minimum radiance for both the window and water vapour channels for the Meteosat 7 data are shown in Fig. 9. Grid points where the amplitude of the diurnal cycle is small have been masked. The colour table in these and subsequent timing plots is cyclic, so that there is no discontinuity around midnight. Over land, the maximum window channel radiance typically occurs close to or just after noon over clear-sky regions and slightly earlier for cloudy regions, in agreement with YS (their Fig. 3(b)). The minimum radiance occurs just before dawn for clear regions, but well into the evening or night where there are significant amounts of cloud. The boundary between these two regimes is well marked over both Africa and South America. As noted earlier, the amplitude of the diurnal cycle in the water vapour channel is much smaller than in the window and the largest values occur where there is deep convection over land. There are, thus, many similarities between the plots for this channel and for the window, with the maxima occurring near or before noon and the minima occurring in the late evening or in the night, when the high clouds are most extensive. As noted by Soden (2000), the two channels thus provide a means for distinguishing the deepest convective clouds, since only these clouds can produce a significant signal in the water vapour channel above the background of water

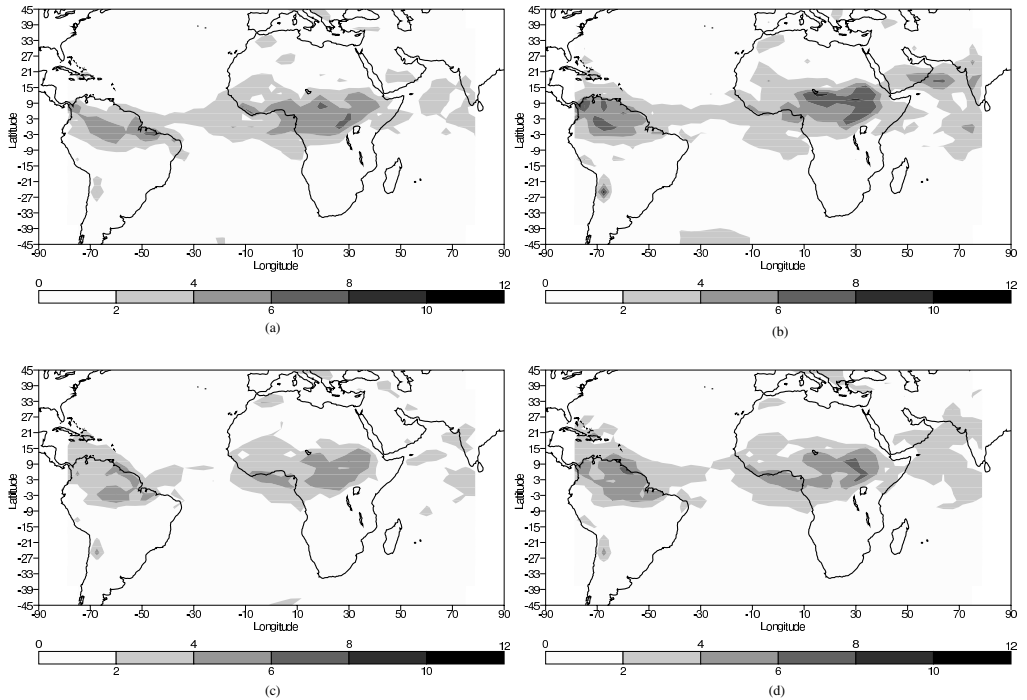


Figure 8. Diurnal range of water vapour channel brightness temperature (K) from the four versions of the model. Panels are as in Fig. 3: (a) 19 levels and calls to the radiation scheme every three hours; (b) 19 levels and calls to the radiation scheme at every time step (half hour); (c) 30 levels and calls every three hours, and (d) 30 levels and calls at every time step (half hour).

vapour emission. For the present study, however, the subsequent analysis will focus on the window channel only, since this captures the main signal of the diurnal cycle in cloudiness in both the satellite data and the model.

Figure 10 shows the local time of maximum window channel radiance for the four versions of the climate model. There is broad agreement with Fig. 9, although there is a tendency for the model maxima to occur somewhat later than in the observations over land lying beneath clear skies ('clear-sky' land). There is no obvious dependence on the vertical or temporal resolution, which disagrees with the finding of YS that increasing the calling frequency of the radiation code led to a 1–2 hour delay in the maximum over the deserts. The difference is believed to be due to the simple method used here to find the time of maximum, since, with three-hourly radiation calls, there are only eight samples per day, so there is an uncertainty in the time of maximum in the control integration which could easily mask a small change of 1–2 hours when more frequent calls are employed. A detailed comparison with the Fourier analysis method of YS is planned for future investigations.

The local time of minimum radiance from the models (Fig. 11) agrees with that from Meteosat 7 (Fig. 9(c)) over clear-sky land, but for cloudy regions there are noticeable departures and also a sensitivity to the calling frequency of the radiation scheme. With the standard three-hour call (the two plots on the left in Fig. 11), the minimum values of radiance (associated with the deepest convective clouds over Africa and South America) occur in the early afternoon, considerably earlier than in the Meteosat data. This is the classic signal of the diurnal cycle error in the modelled

convection, which also holds for the precipitation, as discussed below. In contrast, with the radiation scheme called every time step (the two plots on the right), the South American convection tends to peak even earlier in the day, but over Africa the minimum radiance shifts substantially into the night, bringing the simulation into broad agreement with the observations. While this improvement is to be welcomed, the strong sensitivity to the calling frequency is disconcerting, as it betrays a lack of stability in the response of the model physics to small numerical changes in the radiative forcing.

Figure 12 shows the local time of the precipitation maximum in the models. In common with other climate models, HadAM3 predicts precipitation both from the convection scheme and also from a scheme for ‘large-scale’ condensation (i.e. on the grid scale and above). In the tropics, the bulk of the precipitation comes from the convection scheme, which effectively removes excess moisture before grid-scale saturation can take place. The left hand plots in Fig. 12 show that the tropical precipitation maxima occur in the early afternoon, at about the same time as the minimum radiance. As noted by YS, this indicates a substantial systematic error in the model, since their derived precipitation maxima over land tend to occur well into the evening in most areas of the tropics. It is important to note, however, that more recent and direct estimates of the diurnal cycle of precipitation from Tropical Rainfall Measuring Mission (TRMM) data show the maximum occurring at about 1500h local time over land (Nesbitt and Zipser 2003), much earlier than inferred by YS from the CLAUS data, although still not as early as in the model. It is possible that this indicates a flaw in the methodology used by YS (and many others) to derive information on the diurnal cycle of precipitation from passive infrared radiances. This possibility will be discussed further in Section 6.

With the radiation called every time step (right-hand plots), the model error is exacerbated by a shift in the precipitation maxima to even earlier in the day, for both values of the vertical resolution. Over South America, this maintains the close link between the precipitation and the window channel radiance (i.e. the cloudiness). Over Africa, however, the time of minimum radiance (maximum cloudiness) and maximum precipitation are now completely decoupled from each other, with the former occurring in the middle of the night and the latter in the middle of the day. This extraordinary behaviour is examined further in the following section.

5. MODEL RESULTS FOR SELECTED REGIONS

This section investigates how the model is able to achieve the completely different relationships between the timing of the minimum in the window channel brightness temperature and the maximum in the precipitation over Africa and South America that are evident in the right-hand plots in Figs. 11 and 12. In the interests of brevity, results are presented only from the version of the model with 30 levels and calls to the radiation scheme every time step.

(a) *Africa*

Figure 13 shows area averages of several quantities from the model, plotted against local time, for the African convective region (2.5 to 12.5 degrees North, 15 to 30 degrees East). The downward solar radiation at the top of the atmosphere provides an indication of sunrise and sunset and of the progress of the solar heating through the day. The total cloud amount is calculated by combining the contributions from convective and layer cloud (calculated by the Smith (1990) scheme), taking into account the overlap assumption used in the radiation scheme (clouds in adjacent model layers use the

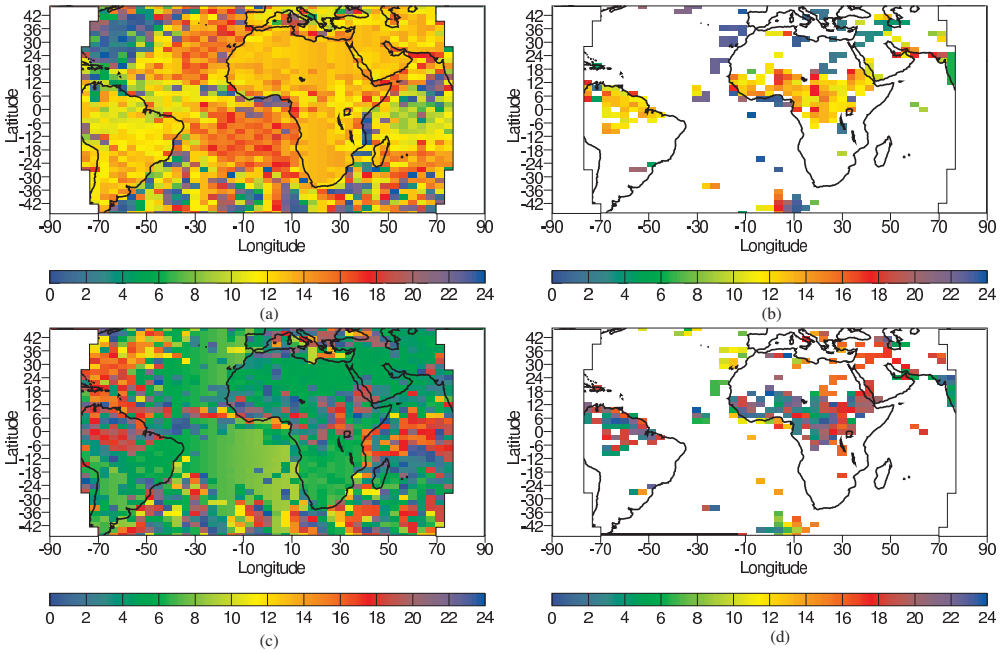


Figure 9. Local time of maximum (upper two panels) and minimum (lower two panels) radiance from Meteostat window channel (left-hand panels) and water vapour channel (right-hand panels). Results are masked to exclude values where the diurnal range is very small.

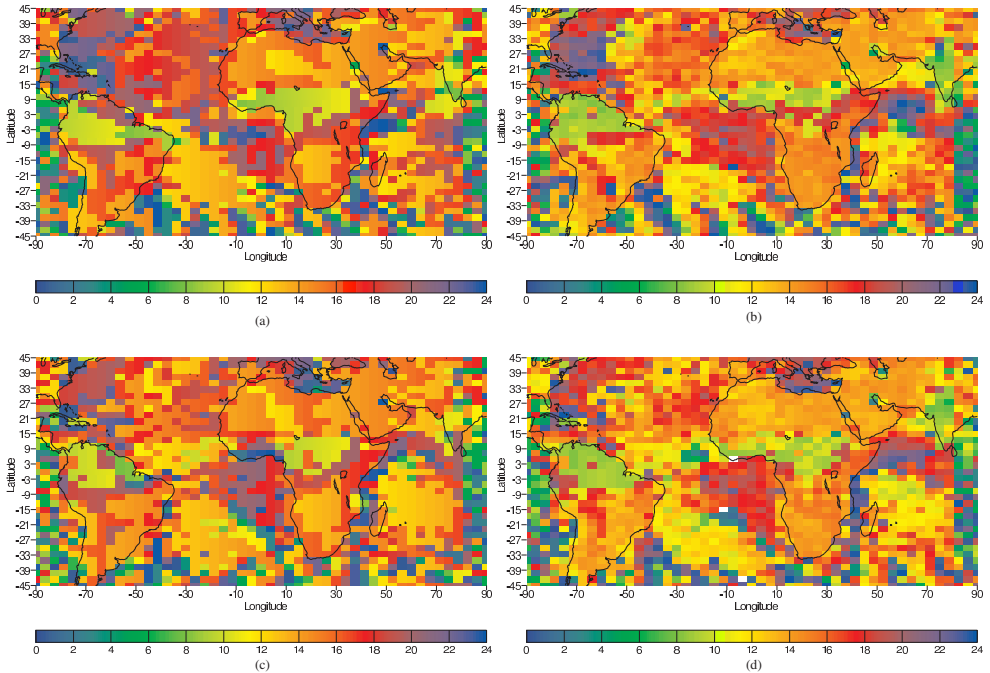


Figure 10. Local time of maximum window channel radiance from the four versions of the model. Panels are as in Fig. 3: (a) 19 levels and calls to the radiation scheme every three hours; (b) 19 levels and calls to the radiation scheme at every time step (half hour); (c) 30 levels and calls every three hours, and (d) 30 levels and calls at every time step (half hour).

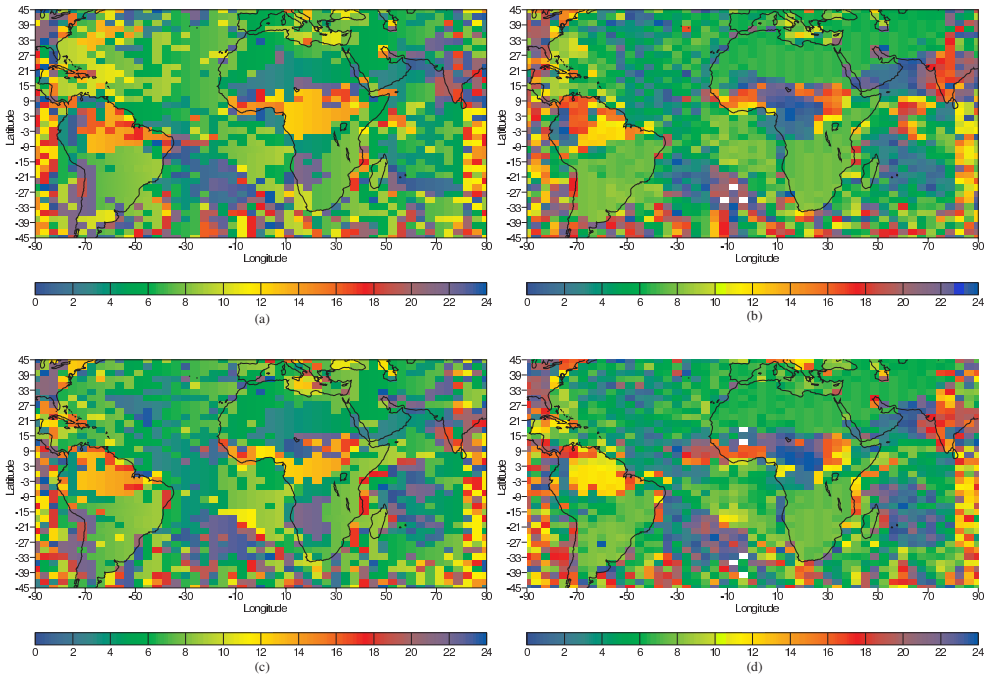


Figure 11. Local time of minimum window channel radiance from the four versions of the model. Panels are as in Fig. 3: (a) 19 levels and calls to the radiation scheme every three hours; (b) 19 levels and calls to the radiation scheme at every time step (half hour); (c) 30 levels and calls every three hours, and (d) 30 levels and calls at every time step (half hour).

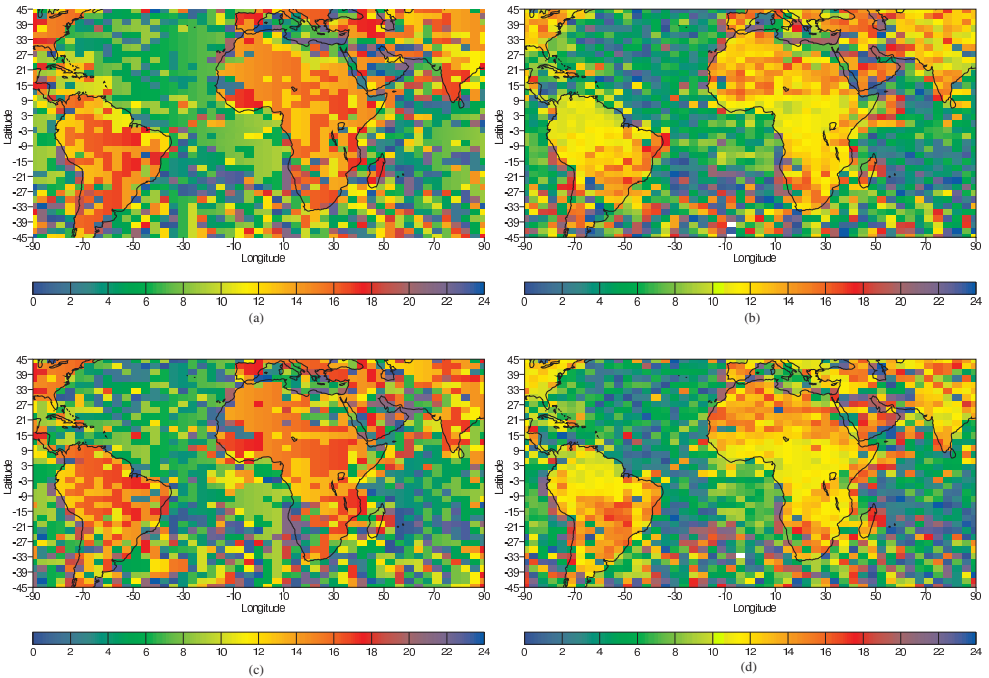


Figure 12. Local time of maximum precipitation from the four versions of the model. Panels are as in Fig. 3: (a) 19 levels and calls to the radiation scheme every three hours; (b) 19 levels and calls to the radiation scheme at every time step (half hour); (c) 30 levels and calls every three hours, and (d) 30 levels and calls at every time step (half hour).

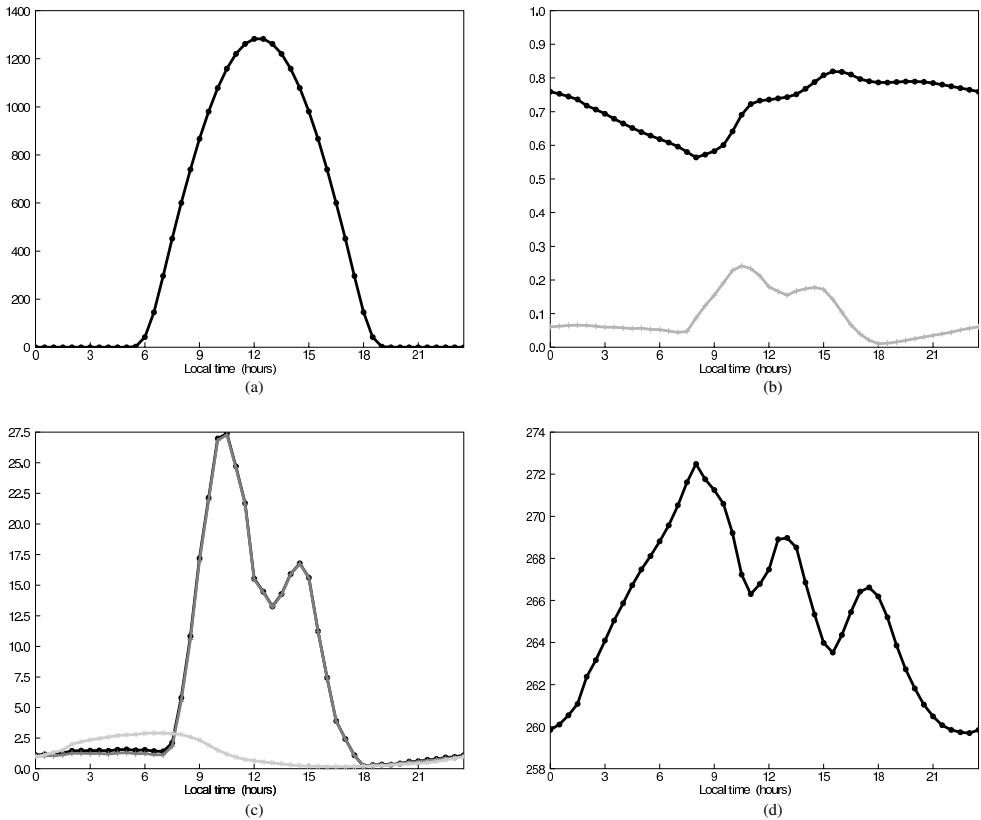


Figure 13. Area averages over central Africa for the boreal summer season (June, July and August) of selected diagnostics from the 30-level version of the model, with half-hourly calls to the radiation scheme, as a function of local time: (a) downward solar radiation at the top of the atmosphere (Wm^{-2}); (b) total cloud fraction (dark) and convective cloud fraction (light); (c) total precipitation (dark), convective precipitation (medium) and large-scale precipitation (light, with values multiplied by ten for clarity) (mm/day), and (d) window channel brightness temperature (K).

maximum overlap assumption, while those separated by one or more layers overlap randomly; convective cloud that occupies more than one layer is vertically coherent and the layer cloud occupies the remaining space in the grid box). Figure 13(c) shows that the convective precipitation dominates the total and that it increases dramatically after sunrise, peaking at about 1000 h local time, consistent with Fig. 12. There is a subsidiary peak in the afternoon, but it then falls to very low values by sunset. The convective cloud amount follows a similar pattern, since it is calculated from the convective mass flux which is related to the precipitation. Figure 14(a) shows the contribution from the convection scheme to atmospheric heating and illustrates that the bulk of the heating is in the mid to upper troposphere, extending to about 200 hPa. Detrainment from the convection scheme moistens the atmosphere and leads to the formation of significant amounts of layer cloud at upper levels, as shown in Fig. 14(b). It is this layer cloud that produces the bulk of the total cloud cover shown in Fig. 13(b). The high cloud reaches a peak in the early evening and then gradually dissipates by dawn. Smaller amounts of layer cloud are apparent at the freezing level at around 630 hPa.

Comparison of Figs. 13(b) and (d) shows that the high-level layer-cloud controls the evolution of the window channel brightness temperature, with a secondary contribution

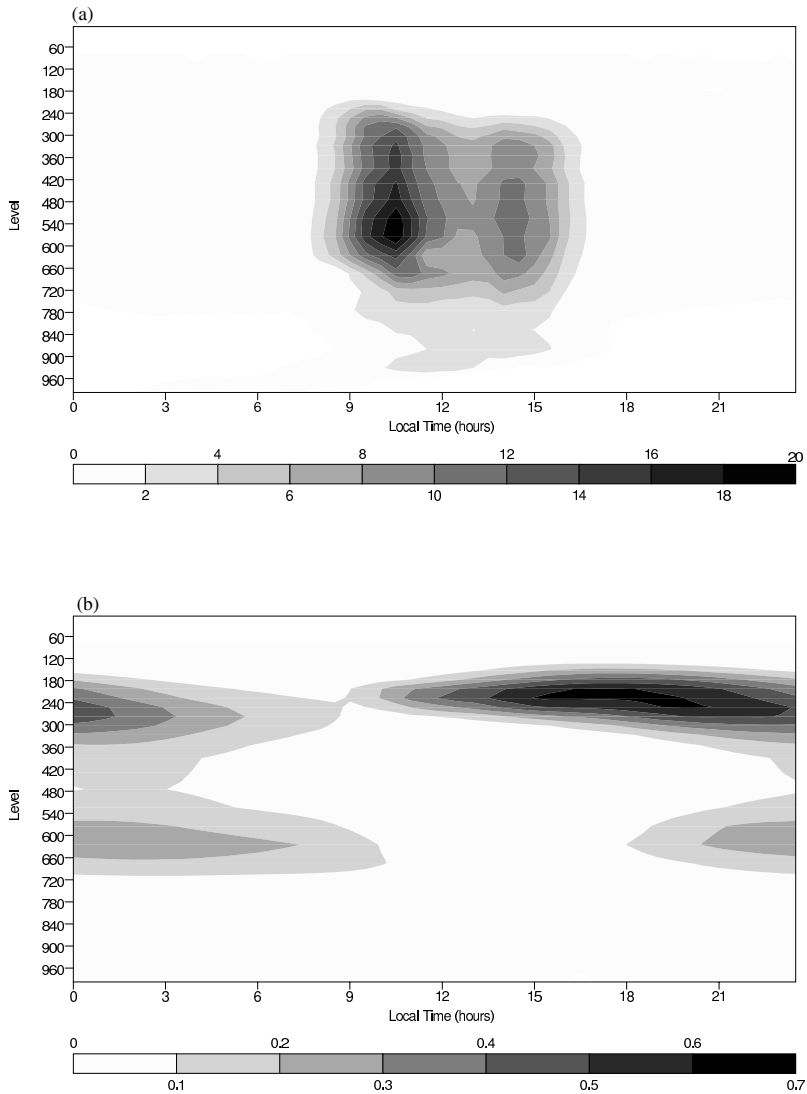


Figure 14. Height–time cross-sections averaged over central Africa for the boreal summer season (June, July and August) from the 30-level version of the model, with half-hour calls to the radiation scheme: (a) convective heating (K/day), and (b) layer cloud fraction.

from the convective cloud. The brightness temperature reaches a minimum just before midnight and then increases as the upper-level cloudiness dissipates, reaching a peak at about 0800 h local time. It then falls as the convective and layer cloud grows, despite increases in surface temperature (not shown). The two minima in the brightness temperature at about 1100 h and 1500 h correspond roughly to the maxima in convective cloudiness, modulated by the layer cloud.

A similar bimodal peak in convection was found by Betts and Jakob (2002) in the ECMWF model. They attributed the first, early morning peak to a failure of the closure

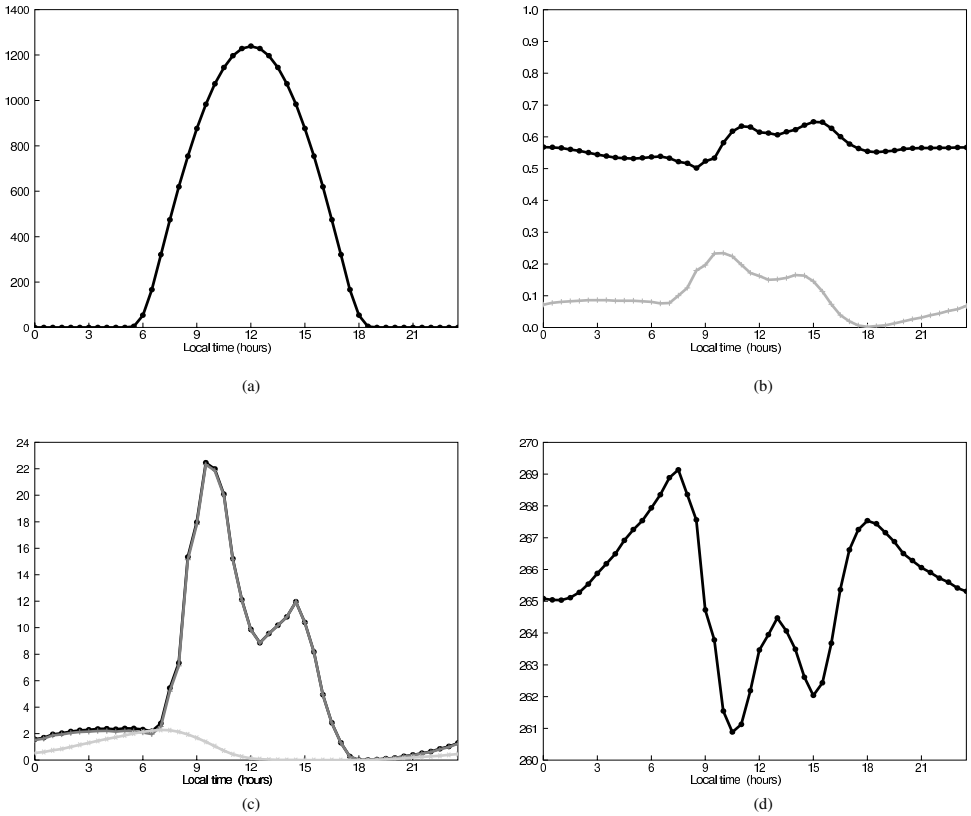


Figure 15. Area averages over South America for the boreal summer season (June, July and August) from the 30-level version of the model, with half-hourly calls to the radiation scheme. Panels are set out as in Fig. 13: (a) downward solar radiation at the top of the atmosphere (Wm^{-2}); (b) total cloud fraction (dark) and convective cloud fraction (light); (c) total precipitation (dark), convective precipitation (medium) and large-scale precipitation (light, with values multiplied by ten for clarity) (mm/day), and (d) window channel brightness temperature (K).

used in the deep convection scheme to respond properly to the breakdown of the night-time stable boundary layer. It is not known whether a similar process occurs in the Hadley Centre model, but it merits further investigation.

These results show that the decoupling between the diurnal cycle of the precipitation and of the window channel brightness temperature occurs because of the growth of significant amounts of upper-level layer-cloud through the day, created by detrainment from the convection. The convective precipitation peaks before noon and dies away by sunset, but the upper-level cloudiness persists and continues to control the window channel brightness temperature, which reaches its minimum about 12 hours after the precipitation maximum.

(b) South America

Figures 15 and 16 show the same diagnostics as in the previous sub-section, but for the South American convective region (5°S to 5°N , 56.25 to 71.25°W). Comparison with Figs. 13 and 14 reveals some important similarities and differences. The behaviour of the convective cloud and precipitation is almost identical to that over Africa, with the main peak just after 0900 h and a secondary maximum in the afternoon. However, the convective heating is much lower down than over Africa, with a peak below the 0°C

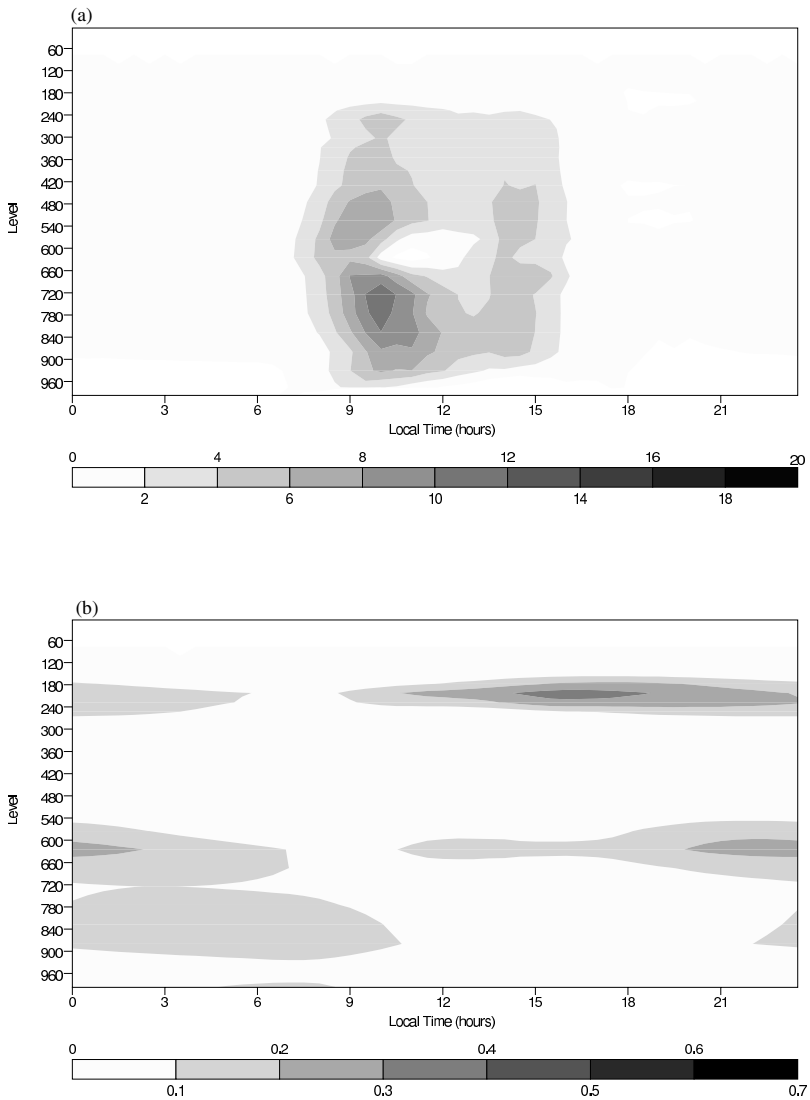


Figure 16. Height–time cross-sections averaged over South America for the boreal summer season (June, July and August) from the 30-level version of the model, with half-hourly calls to the radiation scheme. Panels are set out as in Fig. 14: (a) convective heating (K/day), and (b) layer cloud fraction.

level, which appears as a distinct break in the heating profile (Fig. 16(a)). Consequently, the amount of upper-level layer-cloud is about half that over Africa and is much thinner (Fig. 16(b)). The net result is that the convective cloud has a much greater influence on the window channel brightness temperature, so the minimum brightness temperature now occurs at about 1000 h, just after the maximum in convective cloud and precipitation (Fig. 15).

The differences between the behaviour over Africa and that over South America are thus due to the differences in the strength of the convection in the two regions and the amount of layer cloud created at upper levels from convective detrainment.

The implications of this result for studies of the diurnal cycle of cloudiness, the radiation budget and precipitation are discussed in the final section.

6. DISCUSSION

Simulations of the radiances observed by Meteosat 7 have been used to evaluate the representation of the diurnal cycle in the Hadley Centre climate model, version HadAM3. The study builds on previous investigations by employing a radiance code within the model to simulate directly the satellite radiances, taking into account the viewing geometry and instrument pass band, and by making comparisons for both the infrared window and water vapour channels.

The model produces a good simulation not only of the mean fields but also of the diurnal range of the brightness temperatures for both the window and water vapour channels. Some improvements are also apparent in these fields when either the vertical resolution or the calling frequency of the radiation code is increased, but there are also some negative impacts of improving the numerical resolution. Once the phase of the diurnal cycle is examined, some well known systematic errors emerge that are common to other climate models. Over tropical land, the modelled convective precipitation reaches a maximum before local noon, whereas in reality it peaks much later in the day. The same error is apparent in the time of minimum radiance in the standard configuration of the model with 19 levels and calls to the radiation code every three hours. But when the radiation code is called every model time step (half an hour), the time of minimum radiance shifts to much later in the day, because the model produces large amounts of upper-level cloudiness which persists through the evening and night. Although this brings the radiance diurnal cycle into agreement with the Meteosat data, the precipitation error is still present, so the diurnal cycles of radiance and precipitation are now completely decoupled from each other. In effect, the improvement in the radiance simulation now masks the underlying error in the representation of convection. Since the upper-level cloudiness is itself created by detrainment from the convection scheme, the fundamental error in the model's representation of the diurnal cycle is still present and needs to be corrected.

Although it is dangerous to infer too much from a model with a known large error in the representation of the diurnal cycle, the decoupling between the radiance and precipitation diurnal cycles may have wider implications. The mechanism whereby this decoupling occurs (the establishment of a persistent veil of high cloud well after the convection itself dissipates) appears to be physically plausible. If this mechanism also occurs in the real world, then it could call into question the use of passive infrared satellite measurements to infer the diurnal cycle of precipitation. The established relationships between window channel brightness temperatures and precipitation are based on long-term averages; for example, they contribute to the derived monthly mean diagnostics produced by the Global Precipitation Climatology project (GPCP) (Huffman *et al.* 1997). However, there is no guarantee that these relationships will also hold during the diurnal cycle, when large and coherent changes in cloud structure take place that are not necessarily related directly to the changes in precipitation. It is for this reason that the present study avoids the derivation of precipitation amounts from the radiance data and restricts itself to comparing like with like. Nevertheless, it is clearly important that reliable sources of satellite-based precipitation data should be found that are independent of thermal radiances and which resolve the diurnal cycle. Given that it is impractical to mount active sensors on geostationary satellites, the most practical approach to this problem appears to come from the active and passive microwave sensors

on the TRMM satellite (Negri *et al.* 2002), which is in a low earth orbit that precesses through the diurnal cycle. It is very interesting that recent results on the diurnal cycle of precipitation derived from TRMM data find that the precipitation maximum over land occurs at about 1500 h local time (Nesbitt and Zipser 2003), which is much earlier than found by YS. It is possible that this disagreement is in part due to a similar decoupling to that found in the model and this certainly merits further investigation.

The diurnal cycle errors almost certainly arise from deficiencies in the model's convection scheme. The intention of this work was not to find the source of these deficiencies, but rather to establish a methodology for comparing outputs from the model with data from geostationary satellites, with a view to choosing the optimum resolution in time and space in a future observationally based approach to this and other problems. Future developments of the work include the use of data from the new Meteosat Second Generation (MSG) satellite, which carries an imager with many more infrared channels than the two on Meteosat 7 and also the Geostationary Earth Radiation Budget (GERB) broad-band radiation budget instrument (Schmetz *et al.* 2002). The utility of precipitation data from TRMM for studying the diurnal cycle will also be considered. New versions of the model will be examined, including those with revised parametrizations and further improvements in spatial resolution. Improved horizontal resolution is of particular interest, in order to bring the model's resolution closer to that of the satellite data. This will facilitate the identification of clear-sky regions, enabling the simulation of the diurnal cycle of upper tropospheric water vapour to be investigated.

ACKNOWLEDGEMENTS

Advice from Lois Steenman-Clark, John Edwards and Mark Ringer in porting the radiance version of the model to the Computer Services for Academic Research (CSAR) supercomputers is appreciated. The Meteosat 7 data were obtained from EUMETSAT. The figures were produced using the Visual Climate Data Analysis Tools (VCDAT) package, with helpful advice from Dean Williams at the US Program for Climate Model Diagnosis and Intercomparison. Richard Allan is thanked for comments on the manuscript.

REFERENCES

- | | | |
|---|------|---|
| Allan, R. P., Ringer, M. A. and Slingo, A. | 2003 | Evaluation of moisture in the Hadley Centre climate model using simulations of HIRS water vapour channel radiances. <i>Q. J. R. Meteorol. Soc.</i> , 129 , 3371–3389 |
| Betts, A. K. and Jakob, C. | 2002 | Study of diurnal cycle of convective precipitation over Amazonia using a single column model. <i>J. Geophys. Res.</i> , 107 , 10.1029/2002JD002264 |
| Duvel, J. P. and Kandel, R. S. | 1985 | Regional-scale diurnal variations of outgoing infrared radiation observed by Meteosat. <i>J. Climate Appl. Met.</i> , 24 , 335–349 |
| Gates, W. L., Boyle, J. S., Covey, C., Dease, C. G., Doutriaux, C. M., Drach, R. S., Fiorino, M., Gleckler, P. J., Hnilo, J. J., Marlais, S. M., Phillips, T. J., Potter, G. L., Santer, B. D., Sperber, K. R., Taylor, K. E. and Williams, D. N. | 1999 | An overview of the results of the Atmospheric Model Intercomparison Project (AMIP I). <i>Bull. Amer. Meteorol. Soc.</i> , 80 , 29–56 |
| Gentemann, C. L., Donlon, C. J., Stuart-Menteth, A. and Wentz, F. J. | 2003 | Diurnal signals in satellite sea surface temperature measurements. <i>Geophys. Res. Lett.</i> , 30 , 10.1029/2002GL016291 |

- Hodges, K. I., Chappell, D. W., Robinson, G. J. and Yang, G. 2000 An improved algorithm for generating global window brightness temperatures from multiple satellite infrared imagery. *J. Atmos. Oceanic Technol.*, **17**, 1296–1312
- Huffman, G. J., Adler, R. F., Arkin, P., Chang, A., Ferraro, R., Gruber, A., Janowiak, J., McNab, A., Rudolf, B. and Schneider, U. 1997 The Global Precipitation Climatology Project (GPCP) Combined Precipitation Dataset. *Bull. Amer. Meteorol. Soc.*, **78**, 5–20
- IPCC 2001 *Climate change 2001: the scientific basis*. Houghton, J. T., Ding, Y., Griggs, D. J., Noguer, M., van de Linden, P. J., Dai, X., Maskell, K. and Johnson, C. A. (Eds). Cambridge University Press, Cambridge, UK
- Jakob, C. and Klein, S. A. 1999 The role of vertically varying cloud fraction in the parametrization of microphysical processes in the ECMWF model. *Q. J. R. Meteorol. Soc.*, **125**, 941–965
- Janowiak, J. E., Arkin, P. A. and Morrissey, M. 1994 An examination of the diurnal cycle in oceanic tropical rainfall using satellite and in situ data. *Mon. Weather Rev.*, **122**, 2296–2311
- Lin, X., Randall, D. A. and Fowler, L. D. 2000 Diurnal variability of the hydrologic cycle and radiative fluxes: comparisons between observations and a GCM. *J. Climate*, **13**, 4159–4179
- Morcrette, J.-J. 1991 Evaluation of model-generated cloudiness: satellite-observed and model-generated diurnal variability of brightness temperature. *Mon. Weather Rev.*, **119**, 1205–1224
- Negri, A. J., Bell, T. L. and Xu, L. 2002 Sampling of the diurnal cycle of precipitation using TRMM. *J. Atmos. Oceanic Technol.*, **19**, 1333–1344
- Nesbitt, S. W. and Zipser, E. J. 2003 The diurnal cycle of rainfall and convective intensity according to three years of TRMM measurements. *J. Climate*, **16**, 1456–1475
- Pope, V. D., Gallani, M. L., Rowntree, P. R. and Stratton, R. A. 2000 The impact of new physical parametrizations in the Hadley Centre Climate Model: HadAM3. *Climate Dyn.*, **16**, 123–146
- Pope, V. D., Pammont, J. A., Jackson, D. R. and Slingo, A. 2001 The representation of water vapor and its dependence on vertical resolution in the Hadley Centre Climate Model. *J. Climate*, **14**, 3065–3085
- Randall, D. A., Harshvardhan and Dazlich, D. A. 1991 Diurnal variability of the hydrologic cycle in a general circulation model. *J. Atmos. Sci.*, **48**, 40–62
- Ringer, M. A., Edwards, J. M. and Slingo, A. 2003 Simulation of satellite channel radiances in the Met Office Unified Model. *Q. J. R. Meteorol. Soc.*, **129**, 1169–1190
- Roca, R., Picon, L., Desbois, M., Le Treut, H. and Morcrette, J.-J. 1997 Direct comparison of Meteosat water vapor channel data and general circulation model results. *Geophys. Res. Lett.*, **24**, 147–150
- Schmetz, J., Pili, P., Tjemkes, S., Just, D., Kerkmann, J., Rota, S. and Ratier, A. 2002 An introduction to Meteosat Second Generation (MSG). *Bull. Amer. Meteorol. Soc.*, **83**, 977–992
- Slingo, A., Wilderspin, R. C. and Brentnall, S. J. 1987 Simulation of the diurnal cycle of outgoing longwave radiation with an atmospheric GCM. *Mon. Weather Rev.*, **115**, 1451–1457
- Smith, R. N. B. 1990 A scheme for predicting layer clouds and their water content in a general circulation model. *Q. J. R. Meteorol. Soc.*, **116**, 435–460
- Soden, B. J. 2000 The diurnal cycle of convection, clouds, and water vapor in the tropical upper troposphere. *Geophys. Res. Lett.*, **27**, 2173–2176
- Yang, G.-Y. and Slingo J. 2001 The diurnal cycle in the tropics. *Mon. Weather Rev.*, **129**, 784–801